Crystal structures and electronic properties in the crossover region between the spin-gap system CaV_2O_5 and the linear-chain system NaV_2O_5

Crystal structures and electronic properties in the crossover region between the spin-gap system CaV$_2$O$_5$ and the linear-chain system NaV$_2$O$_5$

Masashige Onoda and Takeo Kagami

Institute of Physics, University of Tsukuba, Tennodai, Tsukuba 305-8571, Japan

Abstract. The structural and electronic properties of the Ca$_{1-x}$Na$_x$V$_2$O$_5$ system, where the composition CaV$_2$O$_5$ exhibits an isolated dimer-like spin-gap state, and NaV$_2$O$_5$ indicates a linear-chain magnetic behaviour and undergoes a spin-singlet transition at $T_c = 34$ K, have been explored by means of x-ray four-circle diffraction and through magnetization and electron paramagnetic resonance measurements. The crystal structures with $0 < x \leqslant 0.1$ and $0.8 \leqslant x \leqslant 1$ are isomorphous with that of CaV$_2$O$_5$, where the space group is $Pmmn$. The effective V valence is correlated with the V–O bond length in the VO$_5$ pyramid, and the transfer integral for the next-nearest-neighbour V–V path is suggested to be larger than those for other paths, which may be consistent with the formation mechanisms of the dimer in the Ca-rich compounds and the V–O–V molecular orbital in the Na-rich compounds. The magnetic properties for $0 < x \leqslant 0.1$ are interpreted as being governed by contributions from the dimer which is formed between the V zigzag chains and from the isolated spins that are present due to the breaking of the dimer. On the other hand, the properties for $0.9 \leqslant x < 1$ still exhibit linear-chain behaviours, and for $x \leqslant 0.97$ the singlet transition with a large reduction of the exchange coupling constant disappears, and no magnetic ordering takes place. The characteristic spin dynamics for the Na-rich compounds is also discussed.

M Supplementary data files are available from the article's abstract page in the online journal; see `www.iop.org`.

1. Introduction

The quantum spin-fluctuation and frustration effects in low-dimensional systems based on 3d-transition-metal ternary oxides have been investigated intensively [1]. Recently, characteristic electronic properties of the CaV$_n$O$_{2n+1}$ insulator system with $n = 2$–4 have been revealed. This system consists of V$_n$O$_{2n+1}$ layers formed by sharing edges and corners of VO$_5$ pyramids, where Ca atoms are situated between the layers, and it has a two-dimensional $S = \frac{1}{2}$ configuration at the V^{4+} (3d^1) site of the [$1/(n + 1)$]-depleted square lattice [2–4]. As an example, the CaV$_2$O$_5$-type structure projected on the ab-plane is shown in figure 1 [4]. CaV$_4$O$_9$ exhibits a singlet ground state with an energy gap of $\Delta \simeq 110$ K which may originate from weakly coupled metaplaquettes [5, 6]. CaV$_2$O$_5$ also exhibits a singlet state with $\Delta \simeq 660$ K basically due to the corner-sharing dimerization between V zigzag chains [4, 7]. On the other hand, CaV$_3$O$_7$ has a stripe-phase magnetic order [8, 9]. Therefore, corner-sharing superexchange interactions for the next-nearest-neighbour V–V path are expected to be very significant for determining the magnetic properties of the CaV$_n$O$_{2n+1}$ system.
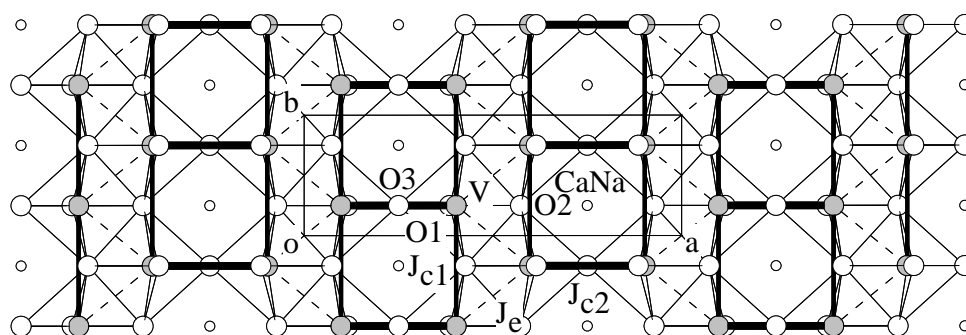
Figure 1. The crystal structure of $Ca_{0.17}Na_{0.83}V_2O_5$ projected onto the *ab*-plane, where the thin lines indicate the edges of the VO_5 pyramids. The broken lines and the thick lines denote the edge-sharing V–V path (J_e) and the corner-sharing ones (J_{c1} and J_{c2}) for the exchange couplings, respectively.

There exist three possible exchange couplings for the CaV_2O_5-type structure (figure 1): J_e, through the edge-sharing path, and J_{c1} (J_{c2}), through the corner-sharing path along the *b*-axis (*a*-axis). As described previously, J_{c2} is rather larger than J_e and J_{c1} for CaV_2O_5 [4, 7]. Moreover, one of the present authors has recently found that $CdVO_3$ has an isolated $S = \frac{1}{2}$ zigzag chain which is almost identical to that of CaV_2O_5, and it is a ferromagnet having J_e equal to -100 K and a Curie temperature of 24 K [10, 11]. The significant difference between the exchange couplings of $CdVO_3$ and CaV_2O_5 is as regards whether J_{c2} exists or not, so these results are consistent with the model with J_e, $J_{c1} \ll J_{c2}$ [4, 7].

The recent structure analysis of NaV_2O_5 indicates that the space group is *Pmmn* with only one equivalent V ion, and charge disproportionation into V^{4+} and V^{5+} ($3d^0$) chains is not allowed, i.e. the V ions are in the state $V^{4.5+}$ [12–14], in contrast to the previous conclusion [15]. In this sense, the NaV_2O_5 structure is similar to the CaV_2O_5-type one shown in figure 1. Since NaV_2O_5 is an insulator and it exhibits one-dimensional $S = \frac{1}{2}$ magnetic properties with an antiferromagnetic exchange coupling constant of 530–560 K [16, 17], it is suggested that spins are not attached to a single V ion, but to a V–O–V molecular orbital between V zigzag chains [12, 18]. In this case, J_{c1} is considered to be the most effective as regards magnetic properties. Moreover, NaV_2O_5 undergoes a spin-singlet transition at $T_c = 34$ K [16] accompanied by a lattice distortion, which has been investigated from various viewpoints [19–23]. There appears to exist a valence ordering from the $V^{4.5+}$ state to the states close to V^{4+} and V^{5+} at around T_c. For example, such a phenomenon, at the temperature of the transition to spin-singlet states, is also seen in other early 3d-transition-metal oxides such as Ti_3O_5 [24, 25]. For NaV_2O_5, several different patterns of the valence order have been postulated [26–32]. In order to obtain direct evidence of the valence order and to clarify which pattern is more appropriate, a full structure determination at temperatures below T_c is very necessary.

Assuming that CaV_2O_5 is a half-filled ladder compound and NaV_2O_5 is a quarter-filled one regardless of J_e, their properties may be discussed from the viewpoints of an isolated rung dimer and a linear chain with a spin of $\frac{1}{2}$ per rung, respectively. It is interesting to explore the crossover between these *extreme* properties through the $Ca_{1-x}Na_xV_2O_5$ system. Section 2 of this paper describes the crystal structures determined by means of single-crystal x-ray diffraction for $Ca_{1-x}Na_xV_2O_5$, and section 3 presents the electronic properties revealed through magnetization and electron paramagnetic resonance (EPR) measurements. Section 4 is devoted to further discussion and conclusions.

2. Crystal structures

Polycrystalline specimens of $Ca_{1-x}Na_xV_2O_5$ with nominal compositions of $x = 0.05, 0.1$, and $0.8 \leqslant x \leqslant 1$ were prepared by heating sealed mixtures of $(1 - x)CaVO_3$, $xNaVO_3$, and VO_2 at temperatures between 958 and 1223 K depending on x. Here, $CaVO_3$ was made according to the method described in reference [33], and VO_2 and $NaVO_3$ were obtained by heating a sealed mixture of V_2O_3 [33] and V_2O_5 at 973 K for 24 h and by heating a mixture of Na_2CO_3 and V_2O_5 at 823 K for 48 h in air, respectively. The large single crystals of NaV_2O_5 and the Ca-doped compound were also prepared by the $NaVO_3$ flux method which is similar to the method described in reference [22].
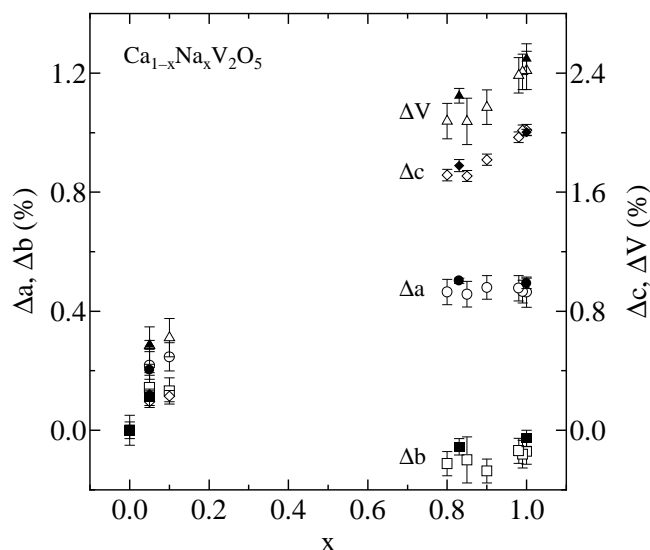

Figure 2. The x-dependences of the lattice constant ratios of $Ca_{1-x}Na_xV_2O_5$, defined as $\Delta p = 1 - p/p_0$, where p is the lattice constant and p_0 is that for CaV_2O_5. The full symbols represent the single-crystal diffraction results.

The single phase for the specimens described above was confirmed on the basis of the x-ray powder diffraction patterns obtained with Cu Kα radiation at 298 K using a Rigaku RAD-IIC diffractometer. For $0.1 < x < 0.8$, the CaV_3O_7-type second phase appeared. Figure 2 shows the x-dependence of the lattice constant ratio defined as $\Delta p = 1 - p/p_0$, where p is the lattice constant and p_0 is that for CaV_2O_5; $a = 11.351(2)$ Å, $b = 3.604(1)$ Å, $c = 4.893(1)$ Å, and $V = 200.2(2)$ Å^3 [4]. The single-crystal diffraction results described below are also plotted, as the full symbols. Only Δc has the linear-in-x dependence, and Δb depends little on x. Although Δa seems to increase with x for the small-x region, it is constant for the large-x region. Thus, the structural dimensionality of the Ca-rich compounds is lower than that of the Na-rich compounds, which is, of course, due to the change of the effective ionic radii of cations as will be discussed in detail later.

The x-ray four-circle diffraction measurements were carried out on a Rigaku AFC-7R diffractometer (custom-made) with graphite-monochromated Mo Kα radiation and an 18 kW rotating-anode generator at 298 K. Here, the single crystals with $x = 0.05$ and 1 used were prepared by the solid-state reaction method, and those with $x = 0.83$ were made by the flux method. As seen later, the structure result for NaV_2O_5 that is presented to allow us to explore the x-dependence of the atomic parameters in the $Ca_{1-x}Na_xV_2O_5$ system is almost consistent

Table 1. Crystal data and a summary of the intensity measurements and refinements for $Ca_{1-x}Na_xV_2O_5$ with $x = 0.05$, 0.83, and 1 at 298 K.

	$Ca_{0.95}Na_{0.05}V_2O_5$	$Ca_{0.17}Na_{0.83}V_2O_5$	NaV_2O_5
a (Å)	11.328(1)	11.294(1)	11.295(2)
b (Å)	3.600(1)	3.606(1)	3.605(1)
c (Å)	4.881(1)	4.806(2)	4.795(1)
V (Å^3)	199.05(6)	195.7(1)	195.2(2)
$\mu_{Mo\,K\alpha}$ (mm^{-1})	5.814	4.982	4.790
D_{cal} (Mg m^{-3})	3.689	3.526	3.485
No of unique reflections	1014	1004	1000
R_{int}	0.051	0.054	0.033
Translation factor	0.71–0.93	0.92–1.00	0.89–1.00
No of observations ($I > 3\sigma$)	731	615	678
No of variables	29	29	28
R	0.039	0.038	0.023
R_w	0.046	0.034	0.019

with that reported recently [12–14]. Intensity data were collected over a maximum 2θ range of 90° using the ω–2θ scan technique and corrections for Lorentz polarization, absorption, and secondary extinction effects were applied. For all of the compounds, the space group and the Z-value were determined to be *Pmmn* (No 59) and $Z = 2$. The lattice constants and the various parameters used for the structure refinements are summarized in table 1.

On the basis of the atomic parameters of CaV_2O_5 [4], the structures were refined by means of full-matrix least-squares calculations with anisotropic displacement parameters. At the same time, the Ca and Na concentrations were determined precisely. Here, the atomic scattering factors were taken from reference [34], and anomalous dispersion effects were included using

Table 2. Atomic coordinates and equivalent isotropic thermal parameters B_{eq} (Å^2) for $Ca_{1-x}Na_xV_2O_5$ with $x = 0.05$, 0.83, and 1 at 298 K, where $y = \frac{1}{4}$ for all of the atoms.

Atom		$Ca_{0.95}Na_{0.05}V_2O_5$	$Ca_{0.17}Na_{0.83}V_2O_5$	NaV_2O_5
V	x	0.40382(5)	0.40241(5)	0.40211(3)
	z	0.3908(1)	0.3913(2)	0.39212(7)
	B_{eq}	0.561(7)	0.738(9)	0.642(4)
Ca, Na	x	$\frac{3}{4}$	$\frac{3}{4}$	$\frac{3}{4}$
	z	0.1559(2)	0.1438(5)	0.1399(3)
	B_{eq}	0.76(1)	1.66(4)	1.41(2)
O1	x	0.3775(2)	0.3852(2)	0.3854(1)
	z	0.0593(5)	0.0573(6)	0.0586(3)
	B_{eq}	1.08(4)	1.18(5)	1.18(2)
O2	x	0.5753(2)	0.5732(2)	0.5731(1)
	z	0.4678(6)	0.4844(7)	0.4878(3)
	B_{eq}	0.77(3)	0.94(5)	0.80(2)
O3	x	$\frac{1}{4}$	$\frac{1}{4}$	$\frac{1}{4}$
	z	0.5453(8)	0.5225(10)	0.5195(4)
	B_{eq}	0.72(4)	0.92(7)	0.78(3)

the values from reference [35]. The final residual factors defined as

$$R = \left(\sum (|F_o| - |F_c|)^2 \right) \Big/ \left(\sum |F_o| \right) \tag{1}$$

$$R_w = \left[\left(\sum w(|F_o| - |F_c|)^2 \right) \Big/ \left(\sum w F_o^2 \right) \right]^{1/2} \tag{2}$$

where F_o and F_c are the observed and calculated structure factors, respectively, are listed in table 1†. All of the calculations were performed using the teXsan crystallographic software package [36].

Table 3. Interatomic distances (Å), angles (deg), V and O valences, and the ground-state wavefunctions for $Ca_{1-x}Na_xV_2O_5$ with $x = 0.05$, 0.83, and 1 at 298 K, where the translation codes are (i) x, y, z; (ii) $1 - x, -y, 1 - z$; (iii) $1 - x, 1 - y, 1 - z$; (iv) $\frac{1}{2} - x, y, z$; (v) $x, -1 + y, z$; (vi) $\frac{1}{2} + x, -y, -z$; (vii) $\frac{1}{2} + x, 1 - y, -z$; (viii) $\frac{3}{2} - x, y, z$.

	$Ca_{0.95}Na_{0.05}V_2O_5$	$Ca_{0.17}Na_{0.83}V_2O_5$	NaV_2O_5
V(i)–O1(i)	1.645(3)	1.617(3)	1.610(1)
V(i)–O2(i)	1.979(2)	1.981(2)	1.985(1)
V(i)–O2(ii, iii)	1.942(1)	1.919(1)	1.9129(7)
V(i)–O3(i)	1.899(2)	1.833(2)	1.8234(8)
O1(i)–O2(i)	2.999(4)	2.954(4)	2.954(2)
O1(i)–O2(ii, iii)	2.975(3)	2.885(4)	2.863(2)
O1(i)–O3(i)	2.778(4)	2.708(5)	2.688(2)
O2(i)–O2(ii, iii)	2.500(3)	2.452(3)	2.448(2)
O3(i)–O2(ii, iii)	2.676(2)	2.691(2)	2.691(1)
V(i)–V(ii, iii)	3.0207(9)	3.034(1)	3.0348(6)
V(i)–V(iv)	3.485(1)	3.443(1)	3.4362(8)
V(i)–O2(ii)–V(ii)	100.78(7)	102.12(7)	102.24(4)
V(i)–O2(ii)–V(v)	135.9(2)	139.9(2)	140.89(8)
V(i)–O3(i)–V(iv)	133.2(2)	139.8(3)	140.9(1)
V(i)–Ca, Na(ii, iii)	3.3424(9)	3.347(2)	3.352(1)
Ca, Na(i)–O1(ii, iii, vi, vii)	2.536(2)	2.553(2)	2.549(1)
Ca, Na(i)–O2(i, viii)	2.497(3)	2.582(3)	2.603(2)
Ca, Na(i)–O3(ii, iii)	2.316(3)	2.413(3)	2.432(2)
V valence	4.08	4.47	4.56
O1 valence	1.58	1.72	1.76
O2 valence	1.79	1.88	1.90
O3 valence	1.42	1.75	1.80
Wavefunction ($r \leqslant 2$ Å)	$0.860d_{xy} - 0.510d_{yz}$	$0.811d_{xy} - 0.585d_{yz}$	$0.795d_{xy} - 0.606d_{yz}$
Wavefunction ($r \leqslant 4$ Å)	$0.993d_{xy} + 0.118d_{yz}$	$0.986d_{xy} + 0.170d_{yz}$	$0.986d_{xy} + 0.169d_{yz}$

The atomic coordinates and equivalent isotropic thermal parameters of $Ca_{1-x}Na_xV_2O_5$ with $x = 0.05$, 0.83, and 1 are listed in table 2. Selected interatomic distances and angles are listed in table 3. Figure 1 shows the crystal structure projected on the *ab*-plane of $Ca_{0.17}Na_{0.83}V_2O_5$. As explained in reference [4], the structures presented here are described in terms of VO_5 pyramids which are linked by sharing edges and corners to form V zigzag chains along the *b*-axis. Along the *a*-axis, these chains are joined by sharing corners, leading to a quasi-two-dimensional layer. Ca and Na atoms are located between the layers and each surrounded by eight O atoms. The displacement parameters for entire atoms are in the normal range.

† Supplementary data files are available from the article's abstract page in the online journal: see http://www.iop.org.

The effective valences at the V and O sites estimated empirically in terms of the bond-length–bond-strength relation [37] are listed in table 3. The V valences almost agree with the values expected from the chemical formula: $4 + x/2$. The ground-state wavefunctions for the VO_5 pyramid are found, on the basis of the crystal fields within the distances r of 2 Å (the pyramid unit only) and 4 Å, to be mainly composed of d_{xy} (table 3), where $x \parallel a$ and $y \parallel b$, using the Hartree–Fock function for V^{4+} [38]. The result that the hole concentrations at the O1 and O3 sites may be higher than that at the O2 site suggests that the transfer integral for the V–O3–V path along the a-axis is larger than those for paths along other directions, as mentioned for NaV_2O_5, on the basis of density-functional theory [12]. Thus, the exchange coupling constant for the V–O3–V path (J_{c2} in figure 1) for the half-filled case is expected to be more effective than J_e and J_{c1}, which is consistent with the mechanism of spin-gap formation in CaV_2O_5 [4, 7].

The average $Ca_{1-x}Na_x$–O distances for the compounds $Ca_{1-x}Na_xO_8$ with $x = 0.05, 0.83$, and 1 are 2.47, 2.52, and 2.53 Å, respectively, which almost agree with the values estimated from reference [39]: 2.50, 2.55, and 2.56 Å with the radius of the oxygen ion being 1.38 Å.

3. Electronic properties

3.1. Magnetic susceptibility

The magnetizations of the polycrystalline specimens with $x = 0.05, 0.1$, and $0.9 \leqslant x \leqslant 1$ were measured by the Faraday method with a field of up to 1 T at temperatures between 4.2 and 850 K. The magnetic susceptibility χ was deduced from the linear part of the magnetization–field (M–H) curve with a decreasing field.

The temperature dependence of the magnetic susceptibility for $Ca_{1-x}Na_xV_2O_5$ with $x = 0.05$ and $0.9 \leqslant x \leqslant 1$ is shown in figure 3(a) and the low-temperature part is indicated in figure 3(b). Apart from the low-temperature parts, the magnetic behaviours for $x = 0.05$ and for $0.9 \leqslant x < 1$ appear to be rather similar to those of CaV_2O_5 and NaV_2O_5, respectively [4, 16].

For $x = 0.05$, there is a rounded maximum at 400 K, while at low temperatures, a Curie–Weiss-like tail possibly due to isolated V^{4+} ions is significant. This result is explained by considering the following contributions: the dimer susceptibility, χ_{dimer}, the Curie–Weiss-type susceptibility of the isolated ions, $\chi_{isolate}$, and the temperature-independent susceptibility of the Van Vleck orbital and diamagnetic components, χ_0:

$$\chi = \chi_{dimer} + \chi_{isolate} + \chi_0 \tag{3}$$

$$\chi_{dimer} = \frac{4C_{dimer}}{T[\exp(\Delta/T) + 3]} \tag{4}$$

$$\chi_{isolate} = \frac{C_{isolate}}{T + T_W} \tag{5}$$

where Δ is the spin gap, C_{dimer} and $C_{isolate}$ are the Curie constants, and T_W is the Weiss temperature. The full curve in figure 3(a) is drawn on the basis of the following parameters: $\Delta = 682.1(4)$ K, $C_{dimer} = 0.3348(6)$ emu K (mol V)$^{-1}$, $C_{isolate} = 7.87(9) \times 10^{-3}$ emu K (mol V)$^{-1}$, $T_W = 2.0(2)$ K, and $\chi_0 = 2.75(8) \times 10^{-5}$ emu (mol V)$^{-1}$. Since the V^{4+} ions in this system have the average g-factor of 1.96 as will be explained later, the above C_{dimer}- and $C_{isolate}$-values are fairly consistent with the values expected from a model wherein the Na or V^{5+} doping gives rise to an unpaired electron which behaves as an isolated spin. The data with $x = 0.1$ (not shown here) are also explained by this idea. The fact that the Δ value obtained here is close to the value for CaV_2O_5 ($\Delta = 667$ K) indicates that the exchange
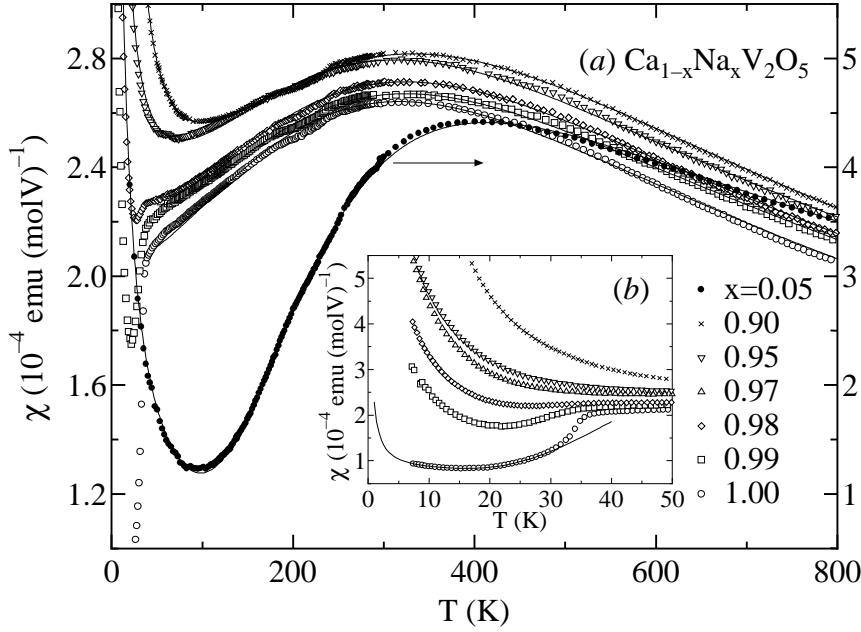
Figure 3. (a) The temperature dependence of the magnetic susceptibility χ of $Ca_{1-x}Na_xV_2O_5$ with $x = 0.05$, 0.9, 0.95, 0.98, 0.99, and 1; (b) the behaviour for $0.9 \leqslant x \leqslant 1$ at temperatures below 50 K. The full curves for $x = 0.05$ and $0.9 \leqslant x \leqslant 1$ in (a) indicate the results calculated from the isolated dimer model and the linear-chain model, respectively, and the curve in (b) is based on the alternating-chain model.

coupling between the zigzag chains depends little on the small degree of doping and that the dimer state of CaV_2O_5 is rather stable. This is the same conclusion as was obtained from the previous investigation for the $CaV_{2-x}Ti_xO_5$ system with $x = 0.1$ and 0.2 in which the Ti ions have no 3d electron [40].

The susceptibility results for $0.9 \leqslant x \leqslant 1$ exhibit broad peaks at around 300 K, as expected for the low-dimensional spin system. These are almost fitted by the relation

$$\chi = \chi_{1d} + \chi_{isolate} + \chi_0 \tag{6}$$

where the first term is the susceptibility for an $S = \frac{1}{2}$ antiferromagnetic Heisenberg chain system [41] and the second term is defined in equation (5). The full curves in figure 3(a) are drawn on the basis of parameters listed in table 4, where C_{1d} and J_{1d} are the Curie constant

Table 4. The susceptibility parameters of the one-dimensional (1d) spins and the isolated ones in paramagnetic regions of $Ca_{1-x}Na_xV_2O_5$; C_{1d} and $C_{isolate}$ are Curie constants (emu K (mol V)$^{-1}$), J_{1d} is the exchange coupling constant (K), T_W is the Weiss temperature (K), and χ_0 is the constant susceptibility (10^{-5} emu (mol V)$^{-1}$).

x	C_{1d}	J_{1d}	$C_{isolate}$	T_W	χ_0
0.90	0.217(1)	541.9(9)	0.00261(4)	$-11.6(6)$	3.84(9)
0.95	0.183(1)	504(1)	0.00172(1)	$-3.97(7)$	6.0(1)
0.98	0.189(1)	510.2(4)	0.00087(1)	0	5.13(4)
0.99	0.181(1)	510.1(7)	0.00083(1)	0	5.56(8)
1.0	0.180(1)	491.0(4)	0.00015(1)	0	4.84(1)

and the exchange coupling constant for χ_{1d}, respectively. The C_{1d}-values nearly correspond to those expected from the chemical formula: $C_{1d} = 0.36(1 - x/2)$ with $g = 1.96$. J_{1d} seems not to depend on x significantly. Since the susceptibility data are well explained in terms of the Heisenberg chain model over a wide temperature region with a reasonable Curie constant, J_{c1} remains the most effective. Thus, it is postulated that the V–O–V molecular orbital still exists for $0.9 \leqslant x < 1$. The previous report of $C_{1d} = 0.188$ emu K $(\mathrm{mol\ V})^{-1}$ and $J_{1d} = 560$ K for $\mathrm{NaV_2O_5}$ exhibiting T_c should be revised [16]. It should be noted that the isolated spin considered here is not intrinsic but due to lattice imperfections and/or defects caused by the doping. No magnetic order exists here except the singlet transitions at T_c.

The singlet transitions at low temperatures are significant just for $0.98 \leqslant x \leqslant 1$, and the transition temperature T_c at which the temperature derivative of χ has a peak decreases with decreasing x: for $x = 1$, $T_c = 34.0$ K, and for $x = 0.99$, $T_c = 29.4$ K. For $x = 0.98$, it is difficult to define T_c precisely, since the susceptibility hollow is not so clear (figure 3(b)). The T_c-value for $\mathrm{NaV_2O_5}$ agrees well with the value reported previously [16]. Various investigations of the magnetic properties at temperatures below T_c for $\mathrm{NaV_2O_5}$ [19, 42–45] have indicated $\Delta_{\mathrm{alter}} = 85$–$101$ K in terms of the alternating exchange model [46]:

$$\chi_{\mathrm{alter}} = \frac{Ng^2\mu_{\mathrm{B}}^2\alpha(\gamma)}{kT}\exp(-J'\beta(\gamma)/T) \tag{7}$$

where N, μ_{B}, and k are the number of spins per mole of V, the Bohr magneton, and the Boltzmann coefficient, respectively, and $\alpha(\gamma)$ and $\beta(\gamma)$ are parameters that are dependent on the alternating parameter γ [47]. However, there was no quantitative discussion that included the prefactor $\alpha(\gamma)$ in equation (7). Let us reanalyse the susceptibility data at temperatures below T_c. As indicated by the full curve in figure 3(b), our data below 30 K are explained by the following parameters: $\gamma = 0.68(1)$, $J' = 291(7)$ K, and $\chi_0 = 7.24(3) \times 10^{-5}$ emu $(\mathrm{mol\ V})^{-1}$, with the same values for χ_{isolate} as are listed in table 4. Therefore, an alternating chain is characterized by the coupling constants 291 and 198 K. Their average is much smaller than the previous value (441 K) [19] and it is reduced to half as compared with $J_{1d} = 491$ K at temperatures above T_c. These parameters give $\Delta_{\mathrm{alter}} = 77$ K from the relation

$$\Delta_{\mathrm{alter}} \simeq \left(\frac{1}{2} + \frac{1}{\pi}\right)(1 - \gamma)J'$$

with a mean-field approximation [48], which is significantly smaller than the value reported previously. Moreover, the χ_0-value is found to be different from the value above T_c as has been pointed out on the basis of NMR investigations [42, 49], which is consistent with the EPR spin susceptibility result described later. It is difficult to explain the change of χ_0 quantitatively. As will be discussed later, the spin–orbit coupling effect itself does not change significantly at around T_c.

3.2. Electron paramagnetic resonance

EPR measurements for the polycrystalline specimens with $x = 0.05$, 0.1, and $0.9 \leqslant x \leqslant 1$ and for the single crystals with $x = 0.83$ and 1 prepared by the flux method were performed at temperatures between 15 and 300 K at 9.2 GHz using a JEOL spectrometer. All of the compounds gave signals with a single Lorentzian and $g \simeq 1.96$ at room temperature. For the single crystals, the measurements were also done as a function of the angle between the direction of the external field and the crystallographic axis in the ac-, bc-, and ab-planes. The spin susceptibility χ_s was extracted precisely on the basis of the integration of the signal, taking account of the temperature dependence of a Q-factor. This paper mainly describes results for the single crystals.

Let us first discuss the results for NaV_2O_5. Although various reports for the EPR investigation of NaV_2O_5 have been published, some disagreements exist there [43–45, 50–52]. Comparing between the χ_s-value and the static susceptibility χ shown in figures 3(a) and 3(b), we can find that χ at temperatures above T_c mainly comes from χ_s, and the χ_0-value changes at around T_c as described earlier. The signal is expressed by a single Lorentzian at temperatures above 18 K. At lower temperatures, the signal is asymmetric due to the superimposition of the signal originating from lattice imperfections and/or defects that are inevitable.

The g-factor for the single Lorentzian basically has the following angular dependence:

$$g = (g_a^2 \cos^2 \phi \sin^2 \theta + g_b^2 \sin^2 \phi \sin^2 \theta + g_c^2 \cos^2 \theta)^{1/2} \tag{8}$$

where θ and ϕ are the polar and azimuthal angles of the direction of the external field, respectively, with respect to the crystallographic axes (a, b, and c) which correspond to the principal axes (X, Y, and Z). Here, g_a depends on the direction of H_1; for example, at 296 K, $g_a = 1.977(1)$ with $H_1 \parallel b$ and $1.974(1)$ with $H_1 \parallel c$. On the other hand, $g_b = 1.974(1)$ with $H_1 \parallel a$ and $1.973(1)$ with $H_1 \parallel c$; and $g_c = 1.936(2)$ with both $H_1 \parallel a$ and $H_1 \parallel b$. This result may be explained by the effect of nondiagonal dynamical susceptibility in the one-dimensional spin system or the so-called dynamical shift [53]. In this case, g_a without the dynamical shift is obtained from $\frac{1}{2}[g_a(H_1 \parallel b) + g_a(H_1 \parallel c)]$. This correction is no more than 0.002, so it is not considered below. Similar phenomena have been observed for CaV_3O_7 and CaV_4O_9 [54].

The temperature dependences of the principal g-factors are shown in figure 4, where g_a, g_b, and g_c are obtained with $H_1 \parallel b$, a, and b, respectively. The relation $g_a \simeq g_b > g_c$ is consistent with the d_{xy}-type ground-state wavefunction for the $V^{4+}O_5$ pyramid expected from the crystal-field analysis. The g-factors are nearly temperature independent at temperatures above T_c,
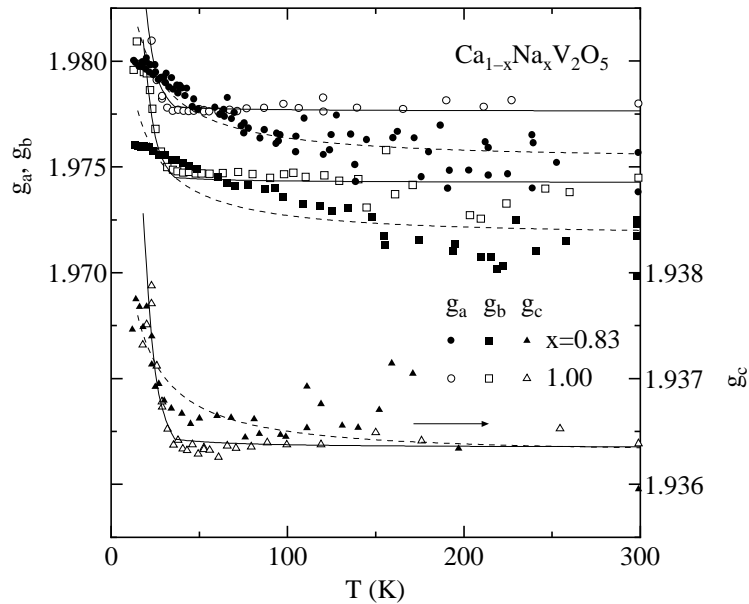

Figure 4. The temperature dependences of the principal g-factors (g_a, g_b, and g_c) of NaV_2O_5 and $Ca_{0.17}Na_{0.83}V_2O_5$, where the crystallographic axes (a, b, and c) correspond to the principal axes (X, Y, and Z), respectively. When the external field is parallel to the a-, b-, and c-axes, the microwave frequency fields are applied parallel to the b-, a-, and b-axes, respectively.

while below T_c, they depend significantly on temperature as described in reference [44]. This is explained by considering that the EPR line originates from the intrinsic spin with parameters g^{int} and χ_s^{int} as well as the impurity spin with parameters g^{imp} and χ_s^{imp}, where χ_s^{imp} is $\chi_{isolate}$ in equation (6), and χ_s^{int} corresponds to χ_{1d} for $T \geqslant T_c$ and χ_{alter} (equation (7)) for $T < 30$ K. Thus, the measured g_i ($i = a$, b, and c) is expected to be given by

$$g_i = \frac{g_i^{int}\chi_s^{int} + g_i^{imp}\chi_s^{imp}}{\chi_s^{int} + \chi_s^{imp}}. \tag{9}$$

The full curves in figure 4 lead to the following parameters: for the intrinsic spin, $g_a^{int} = 1.977$, $g_b^{int} = 1.974$, and $g_c^{int} = 1.936$; for the impurity spin, $g_a^{imp} = 1.985$, $g_b^{imp} = 1.983$, and $g_c^{imp} = 1.939$. The energy level configuration for V^{4+} may be calculated in terms of simple perturbation theory of the spin–orbit coupling [55]:

$$\Delta g_i = 2\lambda \sum_n \frac{|\langle n|L_i|0\rangle|^2}{E_n - E_0} \tag{10}$$

where $\Delta g_i = 2 - g_i$; λ is the spin–orbit coupling constant, L_i is the orbital angular momentum operator, and E_n is the energy of the orbital state n. With $|0\rangle = d_{xy}$, the energies corresponding to the d_{yz}, d_{zx}, and $d_{x^2-y^2}$ states are determined to be 77λ, 87λ, and 125λ, respectively. This level configuration for the excited orbitals is different from that estimated from the crystal-field analysis, in which the first excited orbital is $d_{x^2-y^2}$. This difference is attributable to covalency effects of the oxygen p orbitals.

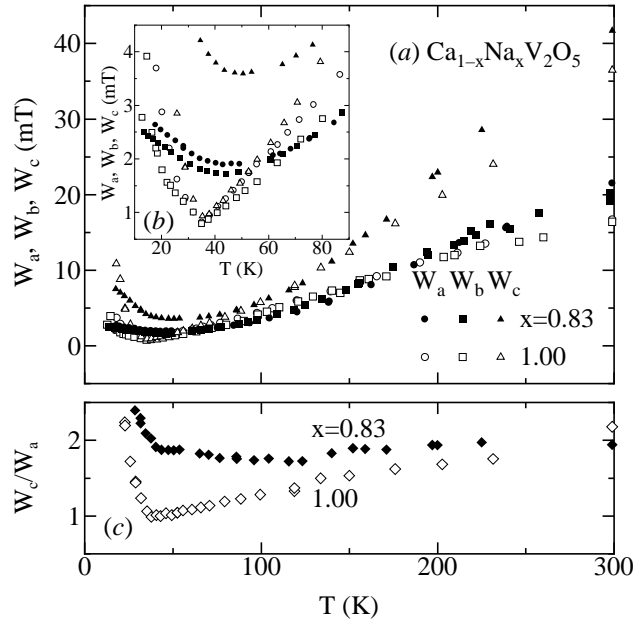The angular dependence of the peak-to-peak linewidth W of the absorption derivative is

Figure 5. (a) The temperature dependences of the principal EPR linewidths (W_a, W_b, and W_c) of NaV_2O_5 and $Ca_{0.17}Na_{0.83}V_2O_5$, where the crystallographic axes (a, b, and c) correspond to the principal axes (X, Y, and Z), respectively; (b) the behaviour at temperatures below 90 K; (c) the results for W_c/W_a.

expressed by

$$W = W_a \cos^2 \phi \sin^2 \theta + W_b \sin^2 \phi \sin^2 \theta + W_c \cos^2 \theta \tag{11}$$

where the definition for θ and ϕ is the same as that in equation (8) and $W_a \simeq W_b$. The temperature dependences of the principal W-values (W_a, W_b, and W_c) are shown in figure 5(a). They decrease monotonically with decreasing temperature at temperatures above T_c, while below T_c, a rapid upturn occurs (figure 5(b)). Here, it should be noted that the ratio, W_c/W_a or W_c/W_b, depends significantly on temperature as shown in figure 5(c). The linewidth is generally a measure of the relaxation rate for spin fluctuations perpendicular to the static field, although its analysis is complicated by the effect of the field on the spin dynamics. For insulating spin systems, there exist several kinds of typical relaxation mechanism through the dipole–dipole (dd) interaction, the anisotropic exchange (ae) interaction, and the Dzyaloshinsky–Moriya (DM) antisymmetric exchange interaction, and so on [55, 56]. Using a correlation time roughly given by $2\hbar/J_{1d}$, $\hbar$ being Planck's constant, the space-averaged linewidth due to the dd interaction is estimated to be $\langle W_{dd} \rangle = 0.08$ mT from the relation

$$\langle W_{dd} \rangle = 2\sqrt{3} g^3 \mu_B^3 J_{1d}^{-1} \sum_{i>j} r_{ij}^{-6}$$

where r_{ij} is the distance between certain spins without consideration of the V–O–V molecular orbital; the width due to the ae interaction is $\langle W_{ae} \rangle = 0.06$ mT from

$$\langle W_{ae} \rangle = 2^{-1} \sqrt{3} \, \Delta g^4 \, g^{-5} \mu_B^{-1} J_{1d}.$$

On the other hand, the width due to the DM interaction, $d_{ij} \cdot (S_i \times S_j)$, with the vector d_{ij} defined between S_i and S_j, is $\langle W_{DM} \rangle \simeq 30$ mT from the relation

$$\langle W_{DM} \rangle = 9^{-1} \sqrt{3} \, \Delta g^2 \, g^{-3} \mu_B^{-1} J_{1d}$$

in the high-temperature limit, where $|d| = 2^{-1} \, \Delta g \, g^{-1} J_{1d}$. This magnitude is comparable to the experimental result. The anisotropy of the linewidth at high temperatures, approximately given by $W \propto 1 + \cos^2 \theta$, is qualitatively explained if, for example, $d_{ij} = (0, 0, d)$ for the third-nearest-neighbour V–V pairs with the exchange coupling of $J_{1d} \simeq J_{c1}$. This d_{ij}-vector is roughly consistent with the anisotropy of the g-factor. The reduction of the anisotropy at low temperatures suggests that another relaxation mechanism in addition to the quantum fluctuation effects has to be considered.

It has been confirmed that the EPR results for the polycrystalline specimens of NaV_2O_5 correspond to the powder patterns calculated with the EPR parameters for the single crystals.

The signal for $Ca_{0.17}Na_{0.83}V_2O_5$ is a single Lorentzian at temperatures above 60 K. At the lower temperatures, the signal seems to consist of two lines with different linewidths and similar g-factors. The angular dependences of the g-factor and the linewidth for the single Lorentzian in the ac-, bc-, and ab-planes are basically given by equations (8) and (11), where their principal axes correspond to the crystallographic axes as in the case of NaV_2O_5. In this compound, the dynamical shift is significant for g_a as well as g_b: at 296 K, $g_a = 1.975(1)$ with $H_1 \parallel b$ and $1.971(1)$ with $H_1 \parallel c$; $g_b = 1.973(1)$ with $H_1 \parallel a$ and $1.969(1)$ with $H_1 \parallel c$; $g_c = 1.936(2)$ with both $H_1 \parallel a$ and $H_1 \parallel b$. It may be difficult to explain this result within the framework of the *purely* one-dimensional spin system. Although the electron distribution would be found on the basis of detailed measurements for the anisotropy of the dynamical shift, it is not touched here. The corrections of the dynamical shift for the measured g are no more than 0.002, and are neglected below. The temperature dependences of the principal g-factors and linewidths are shown in figures 4 and 5(a), respectively, where g_a, g_b, and g_c are obtained with $H_1 \parallel b$, a, and b, respectively. The anisotropy of the g-factor is very similar to that for NaV_2O_5, but its temperature dependence is different, since the present ratio of the impurity

spin to the intrinsic spin may increase with decreasing x as expected from table 4. By analysing the temperature dependence of the g-factor in terms of the same scheme as described earlier with the susceptibility parameters for $x = 0.9$, the following g-factors are obtained with the broken curve in figure 4: for the intrinsic spin, $g_a^{int} = 1.975$, $g_b^{int} = 1.971$, and $g_c^{int} = 1.936$; for the impurity spin, $g_a^{imp} = 1.982$, $g_b^{imp} = 1.978$, and $g_c^{imp} = 1.937$. This result is almost identical to that for NaV_2O_5. At first sight, the temperature dependence of the linewidth seems roughly similar to that for NaV_2O_5, but there is a significant difference: the apparent linewidth has a minimum at about 50 K and then increases *gradually* with decreasing temperature; and the anisotropy of the linewidth is nearly temperature independent for the region where the lineshape is a single Lorentzian. The origin of the linewidth at high temperatures is considered to be similar to that for NaV_2O_5, but the relaxation mechanism at low temperatures is expected to be different.

On the basis of the results for the polycrystalline specimens, it can be said that the rapid upturn of the linewidth at T_c disappears for $x \leqslant 0.97$, which may be consistent with the magnetic susceptibility results.

4. Further discussion and conclusions

To clarify the crossover between the simple dimer-like state of CaV_2O_5 and the linear-chain state of NaV_2O_5, the structural and electronic properties of the $Ca_{1-x}Na_xV_2O_5$ system have been investigated. The single-phase doped compounds have electronic states roughly similar to these two extreme states as summarized below.

The crystal structures for $0 < x \leqslant 0.1$ and $0.8 \leqslant x \leqslant 1$ are isomorphous to that of CaV_2O_5 with only one equivalent V ion. The V valences estimated on the basis of the V–O bond lengths in the VO_5 pyramid are consistent with those expected from the chemical formula.

For the small x-value, the structural properties may lead to a large transfer integral along the V–O3–V path as compared with those along other paths. Thus, the magnetic properties are expected to be mainly determined by the corner-sharing exchange coupling for the next-nearest-neighbour V–V path. In effect, the magnetic properties presented here are interpreted as being governed by contributions from the dimer formed between the zigzag chains and from the isolated spins that are present due to the breaking of the dimer.

The structural consideration for the large x-value suggests that the O3 ion still has a hole concentration larger than that in the O2 ion. Moreover, the V–O3–V bond angle is larger than that for CaV_2O_5. These properties will give a large exchange coupling constant for the V–O3–V path, if spins are attached to a single V ion. However, in order to explain the magnetic and transport properties of NaV_2O_5, we have to consider the V–O3–V molecular orbital as pointed out previously. The compounds with $0.9 \leqslant x < 1$ still indicate linear-chain properties with the effective spin concentrations expected from the chemical formula, so the characteristic molecular orbital is basically unchanged. It is difficult to clarify whether the crossover between the simple dimer-like state and the linear-chain state is continuous or not, since the compounds with $0.1 < x < 0.8$ are not obtained.

The singlet transition disappears for $x \leqslant 0.97$, in which region the compounds remain paramagnetic without any sign of magnetic order. This result is clearly different from the doping effect in the typical linear-chain compound $CuGeO_3$ with a spin–Peierls transition [57]. This difference is probably attributable to the presence of the V–O–V molecular orbital or the freedom of the charge order. The spin-singlet state of NaV_2O_5 is apparently explained in terms of the alternating-chain model with parameters significantly different from those reported previously. The present analysis gives a spin gap smaller than the value determined

by means of the neutron scattering [21]. Therefore, we have to estimate the spin gap using an improved theory, as has been already noted from the large ratio of the gap to T_c. As long as the alternating-chain model is applied, we may expect not complete charge disproportionation into V^{4+} and V^{5+} but incomplete order of V$^{4.5-v}$ and V$^{4.5+v}$ with $0 < v < 0.5$ as suggested in reference [28].

The EPR g-factors and the relaxation mechanism at high temperatures for NaV$_2$O$_5$ and Ca$_{0.17}$Na$_{0.83}$V$_2$O$_5$ are explained within the framework of the usual paramagnetic resonance theory. On the other hand, in order to clarify several characteristics on the relaxation revealed at low temperatures, further considerations are necessary including the effects of the V–O–V molecular orbital, the quantum fluctuations, and the incomplete valence order below T_c.

References

[1] For example, Dagotto E and Rice T M 1996 *Science* **271** 618 and references therein
[2] Bouloux J-C and Galy J 1973 *Acta Crystallogr.* B **29** 1335
[3] Bouloux J-C and Galy J 1973 *Acta Crystallogr.* B **29** 269
[4] Onoda M and Nishiguchi N 1996 *J. Solid State Chem.* **127** 359
[5] Kodama K, Harashina H, Sasaki H, Kobayashi Y, Kasai M, Taniguchi S, Yasui Y, Sato M, Kakurai K, Mori T and Nishi M 1997 *J. Phys. Soc. Japan* **66** 793 and references therein
[6] Fukumoto Y and Oguchi A 1998 *J. Phys. Soc. Japan* **67** 2205 and references therein
[7] Onoda M and Ohyama A 1998 *J. Phys.: Condens. Matter* **10** 1229
[8] Harashina H, Kodama K, Shamoto S, Taniguchi S, Nishikawa T, Sato M, Kakurai K and Nishi M 1996 *J. Phys. Soc. Japan* **65** 1570
[9] Kontani H, Zhitomirsky M E and Ueda K 1996 *J. Phys. Soc. Japan* **65** 1566
[10] Onoda M and Nishiguchi N 1999 *J. Phys.: Condens. Matter* **11** 749
[11] The Heisenberg Hamiltonian is defined as $H = \sum_{\langle i,j \rangle} J S_i \cdot S_j$, S_i being the spin operator at site i.
[12] Smolinski H, Gros C, Weber W, Peuchert U, Roth G, Weiden M and Geibel C 1998 *Phys. Rev. Lett.* **80** 5164
[13] Meetsma A, de Boer J L, Damascelli A and Palstra T T M 1998 *Acta Crystallogr.* C **54** 1558
[14] von Schnering H G, Grin Y, Kaupp M, Somer M, Kremer R K, Jepsen O, Chatterji T and Weiden M 1998 *Z. Kristallogr.—New Cryst. Struct.* **213** 246
[15] Carpy A and Galy J 1975 *Acta Crystallogr.* B **31** 1481
[16] Isobe M and Ueda Y 1996 *J. Phys. Soc. Japan* **65** 1178
[17] Mila F, Millet P and Bonvoisin J 1996 *Phys. Rev.* B **54** 11 925
[18] Horsch P and Mack F 1998 *Eur. Phys. J.* B **5** 367
[19] Weiden M, Hauptmann R, Geibel C, Steglich F, Fischer M, Lemmens P and Güntherodt G 1997 *Z. Phys.* B **103** 1
[20] Fujii Y, Nakao H, Yosihama T, Nishi M, Nakajima K, Kakurai K, Isobe M, Ueda Y and Sawa H 1997 *J. Phys. Soc. Japan* **66** 326
[21] Yosihama T, Nishi M, Nakajima K, Kakurai K, Fujii Y, Isobe M, Kagami C and Ueda Y 1998 *J. Phys. Soc. Japan* **67** 744
[22] Köppen M, Pankert D, Hauptmann R, Lang M, Weiden M, Geibel C and Steglich F 1998 *Phys. Rev.* B **57** 8466
[23] Fertey P, Poirier M, Castonguay M, Jegoudez J and Revcolevschi A 1998 *Phys. Rev.* B **57** 13 698
[24] Onoda M 1998 *J. Solid State Chem.* **136** 67
[25] Onoda M, Ogawa Y and Taki K 1998 *J. Phys.: Condens. Matter* **10** 7003
[26] Seo H and Fukuyama H 1998 *J. Phys. Soc. Japan* **67** 2602
[27] Mostovoy M V and Khomskii D I 1999 *Phys. Rev. Lett.* **82** 976
[28] Gros C and Valenti R 1998 *Preprint* cond-mat/9809154
[29] Thalmeier P and Fulde P 1998 *Europhys. Lett.* **44** 242
[30] Chatterji T, Liß K D, McIntyre G J, Weiden M, Hauptmann R and Geibel C 1998 *Solid State Commun.* **108** 23
[31] Smirnov A I, Popova M N, Sushkov A B, Golubchik S A, Khomskii D I, Mostovoy M V, Vasil'ev A N, Isobe M and Ueda Y 1998 *Preprint* cond-mat/9808165
[32] Lemmens P, Fischer M, Güntherodt G, Mishchenko A S, Weiden M, Hauptmann R, Geibel C and Steglich F 1998 *Phys. Rev.* B **58** 14 159
[33] Onoda M, Ohta H and Nagasawa H 1991 *Solid State Commun.* **79** 281
[34] Cromer D T and Waber J T 1974 *International Tables for X-Ray Crystallography* vol 4, ed J A Ibers and W C Hamilton (Birmingham: Kynoch) section 2

[35] Creagh D C and McAuley W J 1992 *International Tables for Crystallography* vol C, ed A J C Wilson (Boston, MA: Kluwer)

[36] teXsan 1992 *Crystal Structure Analysis Package* (The Woodlands, TX: Molecular Structure Corporation)

[37] Zachariasen W H 1978 *J. Less-Common Met.* **62** 1

[38] Freeman A J and Watson R E 1965 *Magnetism* part A, vol 2, ed G T Rado and H Suhl (New York: Academic)

[39] Shannon R D 1976 *Acta Crystallogr.* A **32** 751

[40] Miyata T, Miura I, Onoda M and Nagasawa H 1993 *48th Annu. Mtg of the Physical Society of Japan* part 3, abstracts (Tokyo: The Physical Society of Japan) p 23 (in Japanese)

[41] Bonner J C and Fisher M E 1964 *Phys. Rev.* **135** A640

[42] Ohama T, Isobe M, Yasuoka H and Ueda Y 1997 *J. Phys. Soc. Japan* **66** 545

[43] Vasil'ev A N, Smirnov A I, Isobe M and Ueda Y 1997 *Phys. Rev.* B **56** 5065

[44] Lohmann M, Loidl A, Klemm M, Obermeier G and Horn S 1997 *Solid State Commun.* **104** 649

[45] Hemberger J, Lohmann M, Nicklas M, Loidl A, Klemm M, Obermeier G and Horn S 1998 *Europhys. Lett.* **42** 661

[46] Bulaevskii N L 1969 *Sov. Phys.–Solid State* **11** 921

[47] Note that γ and J' in equation (7) are sometimes replaced by $(1 - \delta)/(1 + \delta)$ and $(1 + \delta)J''$, respectively, where J'' corresponds to the exchange coupling constant for the uniform chain with $\delta = 0$.

[48] Bray J W, Hart H R Jr, Interrante L V, Jacobs I S, Kasper J S, Watkins G D, Wee S H and Bonner J C 1975 *Phys. Rev. Lett.* **35** 744

[49] Ohama T, Yasuoka H, Isobe M and Ueda Y 1997 *J. Phys. Soc. Japan* **66** 3008

[50] Schmidt S, Palme W, Lüthi B, Weiden M, Hauptmann R and Geibel C 1998 *Phys. Rev.* B **57** 2687

[51] Weiden M, Hauptmann R, Geibel C, Köppen M, Müller J, Lang M, Steglich F, Weiden N, Fischer M, Lemmens P and Güntherodt G 1998 *J. Magn. Magn. Mater.* **177–181** 743

[52] Ogawa K, Onoda M and Nagasawa H 1986 *J. Phys. Soc. Japan* **55** 2129
For this reference, the EPR data were analysed on the assumption of the presence of mobile electrons on the basis of the transport properties reported previously. The absence of T_c for NaV_2O_5 indicates that the Na ions were slightly deficient.

[53] Natsume Y, Sasagawa F, Toyoda M and Yamada I 1980 *J. Phys. Soc. Japan* **48** 50

[54] Taniguchi S, Kobayashi Y, Kasai M, Kodama K and Sato M 1997 *J. Phys. Soc. Japan* **66** 3660

[55] Abragam A and Bleaney B 1970 *Electron Paramagnetic Resonance of Transition Ions* (Oxford: Clarendon)

[56] For example, Yamada I, Nishi M and Akimitsu J 1996 *J. Phys.: Condens. Matter* **8** 2625 and references therein

[57] For example, Fukuyama H, Tanimoto T and Saito M 1996 *J. Phys. Soc. Japan* **65** 1182 and references therein